



## Article

# Role of ACSBG1 in Brain Lipid Metabolism and X-Linked Adrenoleukodystrophy Pathogenesis: Insights from a Knockout Mouse Model

Xiaoli Ye <sup>1,2,†</sup>, Yuanyuan Li <sup>1,3,‡</sup>, Domingo González-Lamuño <sup>1,2,§</sup> , Zhengtong Pei <sup>1,2</sup>, Ann B. Moser <sup>1,2</sup> , Kirby D. Smith <sup>1,3</sup> and Paul A. Watkins <sup>1,2,\*</sup>

<sup>1</sup> Hugo W. Moser Research Institute at Kennedy Krieger, Baltimore, MD 21205, USA

<sup>2</sup> Department of Neurology, Johns Hopkins University School of Medicine, Baltimore, MD 21205, USA

<sup>3</sup> Department of Genetic Medicine and the McKusick-Nathans Institute of Genetic Medicine, Johns Hopkins University School of Medicine, Baltimore, MD 21205, USA

\* Correspondence: watkins@kennedykrieger.org; Tel.: +1-443-923-2754; Fax: +1-443-923-2755

† Current address: School of Life Sciences, Southwest University, Chongqing 400715, China.

‡ Current address: Montefiore Medical Center, Albert Einstein College of Medicine, Bronx, NY 10467, USA.

§ Current address: Pediatra, Unidad de Nefrología y Metabolismo Infantil, Hospital U. Marqués de Valdecilla, 39008 Santander, Spain.

**Abstract:** “Bubblegum” acyl-CoA synthetase (ACSBG1) is a pivotal player in lipid metabolism during mouse brain development, facilitating the activation of long-chain fatty acids (LCFA) and their incorporation into lipid species that are crucial for brain function. ACSBG1 converts LCFA into acyl-CoA derivatives, supporting vital metabolic processes. Fruit fly mutants lacking ACSBG1 exhibited neurodegeneration and had elevated levels of very long-chain fatty acids (VLCFA), characteristics of human X-linked adrenoleukodystrophy (XALD). To explore ACSBG1’s function and potential as a therapeutic target in XALD, we created an ACSBG1 knockout (*Acsbg1*<sup>−/−</sup>) mouse and examined the effects on brain FA metabolism during development. Phenotypically, *Acsbg1*<sup>−/−</sup> mice resembled wild type (w.t.) mice. ACSBG1 expression was found mainly in tissue affected pathologically in XALD, namely the brain, adrenal gland and testis. ACSBG1 depletion did not significantly reduce the total ACS enzyme activity in these tissue types. In adult mouse brain, ACSBG1 expression was highest in the cerebellum; the low levels detected during the first week of life dramatically increased thereafter. Unexpectedly, lower, rather than higher, saturated VLCFA levels were found in cerebella from *Acsbg1*<sup>−/−</sup> vs. w.t. mice, especially after one week of age. Developmental changes in monounsaturated ω9 FA and polyunsaturated ω3 FA levels also differed between w.t. and *Acsbg1*<sup>−/−</sup> mice. ACSBG1 deficiency impacted the developmental expression of several cerebellar FA metabolism enzymes, including those required for the synthesis of ω3 polyunsaturated FA, precursors of bioactive signaling molecules like eicosanoids and docosanoids. These changes in membrane lipid FA composition likely affect membrane fluidity and may thus influence the body’s response to inflammation. We conclude that, despite compelling circumstantial evidence, it is unlikely that ACSBG1 directly contributes to the pathology of XALD, decreasing its potential as a therapeutic target. Instead, the effects of ACSBG1 knockout on processes regulated by eicosanoids and/or docosanoids should be further investigated.

**Keywords:** ACSBG1; bubblegum; X-linked adrenoleukodystrophy; very long-chain fatty acid; brain fatty acid levels; eicosanoids and docosanoids; inflammation; membrane fluidity



**Citation:** Ye, X.; Li, Y.; González-Lamuño, D.; Pei, Z.; Moser, A.B.; Smith, K.D.; Watkins, P.A. Role of ACSBG1 in Brain Lipid Metabolism and X-Linked Adrenoleukodystrophy Pathogenesis: Insights from a Knockout Mouse Model. *Cells* **2024**, *13*, 1687. <https://doi.org/10.3390/cells13201687>

Academic Editor: Gérard Lizard

Received: 26 August 2024

Revised: 4 October 2024

Accepted: 8 October 2024

Published: 12 October 2024



**Copyright:** © 2024 by the authors. Licensee MDPI, Basel, Switzerland. This article is an open access article distributed under the terms and conditions of the Creative Commons Attribution (CC BY) license (<https://creativecommons.org/licenses/by/4.0/>).

## 1. Introduction

Fatty acids (FA) are the building blocks of complex lipids, including triacylglycerol, glycerophospholipids, sphingolipids and cholesterol esters. Fatty acids are also an indispensable metabolic fuel when degraded by β-oxidation. To participate in either anabolic or

catabolic pathways, fatty acids must first be activated by thioesterification to coenzyme A (CoA), a reaction catalyzed by members of the fatty acyl-CoA synthetase (ACS) family (EC 3.4.1.x) [1,2]. Phylogenetic analysis revealed that most human and mouse ACSs segregate into subfamilies that roughly correlate with their FA substrate chain length preference; thus, short- (ACSS), medium- (ACSM), long- (ACSL) and very long-chain (ACSVL) ACSs have been described [2]. Human and mouse homologs of the gene disrupted in the *Drosophila melanogaster* “*bubblegum*” mutant were the basis for the identification of an additional ACS family, designated ACSBG [3]. In addition to differences in their FA chain length preference, ACSs also differ in their tissue, cell and subcellular locations [1]. Most tissue types and cells express several ACSs. For example, proteomics indicated that brain astrocytes express at least 7 of the 14 ACSs that constitute the ACSL, ACSVL, and ACSBG families [PAW, unpublished observation]. These observations suggest that individual ACSs must play unique and specific roles in lipid metabolism.

Several inherited neurologic disorders, particularly the leukodystrophies, are associated with abnormal FA metabolism. In X-linked adrenoleukodystrophy (XALD), deficient degradation of saturated very long-chain FA (VLCFA) in peroxisomes results in elevated levels of these FA, and, in particular, C26:0, in plasma and tissues [4]. Early hypotheses predicted that the defective synthesis of VLCFA-CoA by a peroxisomal very long-chain ACS was the cause of XALD [5,6]. The discovery of the gene mutated in XALD, ABCD1, largely disproved this hypothesis [7]. ABCD1 is an ATP-binding cassette half-transporter and is predicted to homodimerize in the peroxisomal membrane to form a functional transport molecule [8]. Subsequent investigation revealed that ABCD1 does not transport VLCFA, but rather VLCFA-CoA [9–11].

There are two major phenotypic presentations of XALD in males—the childhood cerebral form (CCER) and the adult-onset peripheral neuropathy, adrenomyeloneuropathy (AMN) [4]. Both CCER and AMN are caused by mutations in ABCD1, and both phenotypes can often be present in members of the same nuclear family. In CCER, which affects about 35% of patients, symptoms typically appear around 7 years of age. Inflammatory demyelination usually leads to death by 4 years following the onset of cerebral symptoms. In AMN, which affects more than 60% of patients, the brain is generally spared, but a dying back of long axons of spinal cord neurons leads to a disturbance in gait, as well as effects on bowel and bladder function. Females heterozygous for a pathogenic mutation in ABCD1 are XALD carriers, and many develop peripheral neuropathy resembling AMN as they grow older. However, while almost all male XALD patients develop adrenal insufficiency (Addison’s disease) that typically predates neurologic symptoms, adrenal involvement is rare in heterozygous women. Testicular insufficiency is frequently seen in male AMN patients. Thus, the primary organs affected in XALD are the brain and nerves, adrenal glands and testis. Since ABCD1 is expressed in most tissues (Figure S1), the question arises as to why mutations have pathologic consequences in only a few tissue types. Of potential significance is the fact that brain expression of ABCD1 is among the lowest of 27 tissues examined, while adrenal and testis expression are among the highest (Figure S1).

Although abnormal activation of VLCFA is thus not causative of XALD pathology, the nature of the specific ACS that activates these FA prior to transport, particularly in the tissues pathologically affected in this disorder, has not been determined. Among the ACSs that are potential candidate activators of VLCFA, one enzyme of potential interest is ACSBG1. This enzyme has been characterized in humans [12,13] and mice [14,15] and is also expressed in many other organisms [16].

We [12,13] and others [14] have reported that ACSBG1 expression is primarily found in the brain, adrenal gland, testis and ovary. Deficiency of the ACSBG1 homolog *bubblegum* in *Drosophila melanogaster* led to adult neurodegeneration, with marked dilation of photoreceptor axons and elevated levels of VLCFA [3]. To gain further insights into the potential role of ACSBG1 in FA metabolism, and to assess its potential as a therapeutic target in XALD, we produced an ACSBG1 knockout (*Acsbg1*<sup>−/−</sup>) mouse. In this report, we examine the potential role of ACSBG1 in lipid metabolism in the developing mouse brain. Despite

compelling circumstantial evidence implicating ACSBG1 in XALD pathophysiology, we conclude that a direct role is unlikely. Rather, eicosanoid- and docosanoid-mediated indirect effects of ACSBG1 in XALD should be investigated further.

## 2. Materials and Methods

### 2.1. Materials and General Methods

An affinity-purified antibody to human ACSBG1 was prepared as described previously [13]. The sources of commercial primary antibodies were as follows: GAPDH (Sigma-Aldrich, St. Louis, MO, USA), ACC1 (Cell Signaling, Danvers, MA, USA), FASN (Cell Signaling, Danvers, MA, USA). Secondary antibodies were from Jackson ImmunoResearch (West Grove, PA, USA). Protein was measured using the Pierce 660 nm protein assay kit (Thermo Scientific, Waltham, MA, USA), according to the manufacturer's protocol. [1-14C]palmitic acid (C16:0) and [1-14C]lignoceric acid (C24:0) were from Moravsek Inc. (LaBrea, CA, USA). The ACS activity in mouse tissue was measured as described previously [17]. RNA-seq data for the estimation of ABCD1 expression in 27 human tissue types were obtained through the National Center for Biotechnology Information (NCBI) portal [18] and are shown in Figure S1.

### 2.2. Animals and Their Care

Mice (strain 129vev) were obtained from Taconic Biosciences. All animal studies were approved by the Johns Hopkins University School of Medicine Institutional Animal Care and Use Committee (IACUC), in accordance with the guidelines and regulations described in the NIH Guide for the Care and Use of Laboratory Animals. Wild-type (w.t.) and *Acsbg1* knockout mice (*Acsbg1*<sup>-/-</sup>) were housed in the animal facility of Johns Hopkins School of Medicine under a 12 h light/dark cycle with ad libitum access to food and water. The facility was pathogen-free and was maintained at a constant temperature (22 °C). Animals were sacrificed by asphyxiation with CO<sub>2</sub> and decapitated at postnatal day 1, 4, 8, 15, 30, 60, 120 and 180. Brains were removed and frozen quickly in liquid nitrogen. Whole brain or brain regions were homogenized in 0.25 M sucrose containing 10 mM Tris pH 8.8 and 1 mM EDTA (STE) using a hand-driven pestle. Homogenates were analyzed for specific protein expression (Western blot), mRNA expression (qRT-PCR) and FA analysis (GC-MS) as described below.

### 2.3. Production of an ACSBG1 Knockout Mouse (*Acsbg1*<sup>-/-</sup>)

*Acsbg1*<sup>-/-</sup> mice were produced by targeted disruption of exon 2 (encoding amino acid 40–73) of murine *Acsbg1* (accession # NP\_444408; reference sequence NM\_053178). Genomic sequences 5' and 3' of *Acsbg1* exon 2 were amplified from a mouse genomic bacterial artificial chromosome (BAC) clone (Genome Systems, Inc., St. Louis, MO, USA; RPCI-22) containing the *Acsbg1* gene from mouse strain 129vev (Taconic Biosciences, Albany, NY, USA). The amplified genomic sequences were sequentially cloned into a vector (ploxpsaβgalneo) containing β-galactosidase cDNA and a neomycin resistance cassette (Figure 1A). After confirming the clone orientation by restriction enzyme digestion and DNA sequencing, this plasmid was linearized with Not I and used for transfection of mouse embryonic stem (ES) cells derived from strain 129vev. Individual colonies resistant to growth in culture medium containing the antibiotic G418 (geneticin) were tested for targeted homologous recombination by Southern blot analysis. A schematic of the *Acsbg1* gene structure in wild type ES cells and after homologous recombination of mutated exon 2 in the target allele is shown in Figure 1A. The positions of the BamH1 restriction enzyme site and the probe for Southern blotting (316 bp) are indicated. Transfected ES cell DNA was digested with BamH1, transferred to a membrane and hybridized with a probe for exon 1. The predicted sizes of the wild type and disrupted *Acsbg1* allele were 7 Kb and 4 Kb, respectively. A representative blot is shown in Figure 1B. Examination of 150 clones identified 12 with targeted disruption of the *Acsbg1* gene. PCR analysis of the insertions confirmed that they were in the proper orientation, i.e., downstream of the *Acsbg1* pro-

moter. Cytological analysis revealed 5 clones with normal karyotypes, and 4 were used for blastocyst injection. There were 12 chimeras identified on the basis of coat color among the resulting pups. Backcrossing to Blk6 demonstrated that 4 of the chimeras had germline transmission. *Acsbg1* heterozygotes were obtained from 2 independent chimeras, and *Acsbg1*<sup>-/-</sup> homozygotes were generated by brother–sister mating. Homozygosity for the disrupted *Acsbg1* gene was established by PCR and Southern blot analyses.

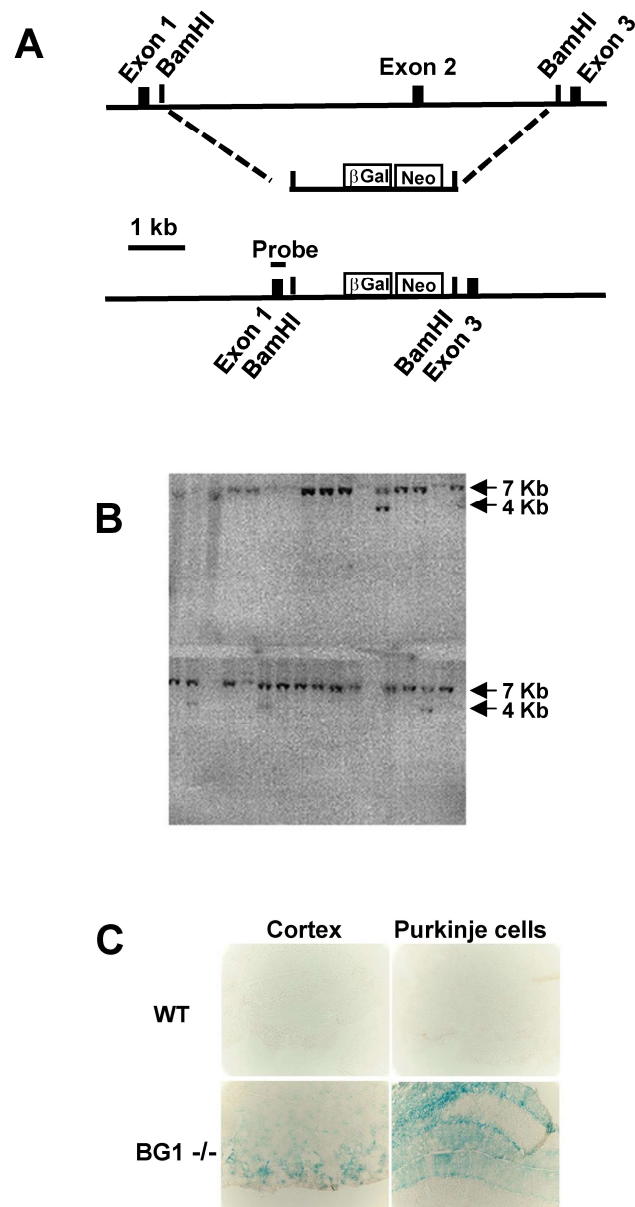


**Figure 1.** Production of an ACSBG1-deficient (*Acsbg1*<sup>-/-</sup>) mouse. (A) w.t. and knockout (KO) constructs. Genomic sequences 5' and 3' of *Acsbg1* (mBG) exon 2 amplified from a mouse genomic bacterial artificial chromosome were sequentially cloned into a vector containing  $\beta$ -galactosidase cDNA and a neomycin resistance cassette. (B) Southern blot analysis. Mouse embryonic stem (ES) cells were transfected with the linearized KO plasmid. G418-resistant colonies were tested for targeted homologous recombination by Southern blot analysis using a probe for exon 1. The predicted sizes of w.t. and KO alleles are 7 Kb and 4 Kb, respectively. (C)  $\beta$ -Galactosidase expression. Paraformaldehyde-fixed sections of the cerebral cortex and cerebellum from w.t. and *Acsbg1*<sup>-/-</sup> (*BG1*<sup>-/-</sup>) mice were incubated for 2 h in X-gal. Cortical neurons and cerebellar Purkinje cells expressing the KO construct stained blue.

## 2.4. Quantitative Real-Time PCR Assay

Total RNA was extracted from the homogenized cerebella of WT and *Acsbg1*<sup>-/-</sup> mice using the TRIzol<sup>®</sup> Reagent (Invitrogen, USA), following the manufacturer's protocol. The total RNA concentration was determined using a NanoDrop 2000 spectrophotometer (Thermo Scientific, USA). Total RNA (3 µg/each reaction) was reverse-transcribed into first-strand cDNA using the SuperScript III First-Strand Synthesis System for RT-PCR kit (Invitrogen, USA), following the manufacturer's protocol, on a Bio-Rad PCR instrument (Bio-Rad, USA). Samples were heated at 65 °C for 5 min, 50 °C for 50 min and then 85 °C for 5 min. Then, 1 µL of RNase H was added to each tube, followed by incubation for 20 min at 37 °C. Polymerase chain reaction (PCR) with Taq Polymerase (Invitrogen, USA) was performed using gene-specific primers, designed using Primer 3.0 (Version 0.4.0) software (Table 1). The qRT-PCR reaction with 5 µL cDNA (4 ng/µL) and 7.5 µL SYBR<sup>®</sup>Green PCR Master Mix (5 µL) (Applied Biosystems) was performed on a Bio-Rad CFX Connect real-time system (Bio-Rad, USA). After 3 min at 95 °C, samples were cycled at 95 °C for 10 s, 55 °C for 10 s and 72 °C for 30 s for 40 cycles; for melt curves, the sample temperature was increased from 55.0 °C to 95.0 °C at 0.5 °C intervals for 5 s each. The *GAPDH* gene was amplified in the same experiment to serve as the reference gene, and the mRNA expression levels were normalized to those of *GAPDH* [19].

**Table 1.** Primer sequences for genes studied.

Gene	NCBI Reference Sequence	Size (bp)	Forward Primer (5'-3')	Reverse Primer (5'-3')
<i>Acsbg1</i>	NM_053178.2	168	catgtccagcccatacaact	atggcctcacaggtttgtc
<i>Acc1</i>	NM_133360.2	239	gcctcttcctgacaaaacgag	tgactgccgaaacatctctg
<i>Acc2</i>	NM_133904.2	217	accgactgaaggacatacgg	acgctgaagtaacccacac
<i>Fasn</i>	NM_007988.3	158	tgggttctagccagcagagt	accaccagagacggttatgc
<i>Fads1</i>	NM_146094.2	177	aagcacatgccatacaacca	cagcggcatgtaagtgaaga
<i>Fads2</i>	NM_019699.1	152	gctctcagatcaccgaggac	agtgccgaagtacgagagga
<i>Elovl2</i>	NM_054326.1	148	tcgacagtgcaggagaaggta	cgctgggtgatagacatgaagg
<i>Elovl5</i>	NM_068801.1	112	ggtggctgttcttcagattgg	cttcaggtggtcttctccga
<i>Gapdh</i>	NM_008084.2	223	aacttggcattgtggaagg	acacattggggtaggaaca

## 2.5. Lipid Analysis by GC/MS

Fresh cerebellum was harvested from mice (WT and *Acsbg1*<sup>-/-</sup>) (n = 5) of different ages (1, 4, 8, 15, 50, 120 and 180 days) and homogenized in STE using a hand-driven pestle. Total fatty acyl groups from 1 mg cerebellar protein were quantitated as their pentafluorobenzyl bromide derivatives on a capillary gas chromatography–electron capture negative-ion mass spectrometry (GC/MS) system (Agilent, Santa Clara, CA, USA) with a Supelco SP2560 capillary column (50 m × 0.25 mm × 0.2 µm), as previously described [20]. Results are expressed as the percentage of total FA detected in the sample.

## 2.6. Electrophoresis and Western Blotting

Brain or cerebellum from mice of different ages was homogenized in STE (pH 8.0) supplemented with protease inhibitors (Roche, Indianapolis, IN, USA) and proteins separated by SDS/PAGE. Proteins were transferred to PVDF membranes and analyzed by Western blotting. After blocking with 10% milk for 1 h at room temperature, the membranes were incubated overnight at 4 °C with primary antibody, followed by secondary antibody for 1 h. Primary antibodies used for Western blotting were as follows: anti-rabbit ACSBG1 (1:200); anti-rabbit acetyl-CoA carboxylase (ACC1, 1:4000); anti-rabbit fatty acid synthase (FASN, 1:4000); anti-mouse glyceraldehyde-3-phosphate dehydrogenase (GAPDH, 1:20,000). Secondary antibodies: goat anti-rabbit horseradish peroxidase (HRP, 1:8000); goat anti-chicken HRP (1:4000); goat anti-mouse HRP (1:8000).

## 2.7. Statistical Analysis

The statistical significance of differences in the biochemical parameters measured in wild-type and *Acsbg1*<sup>-/-</sup> mice with different ages was determined by Bonferroni's

mean comparison test (one-way ANOVA) and two-sample Student's *t*-tests.  $p < 0.05$  was considered statistically significant.

### 3. Results

#### 3.1. Production and Characterization of an *Acsbg1* Knockout (*Acsbg1*<sup>-/-</sup>) Mouse

To elucidate the physiological functions of “bubblegum” (ACSBG1), we produced a knockout (KO; *Acsbg1*<sup>-/-</sup>) mouse by targeted disruption of exon 2 (encoding amino acids 40–73), as described in Materials and Methods. Mice were bred to homozygosity and maintained by mating of *Acsbg1*<sup>-/-</sup> males with *Acsbg1*<sup>-/-</sup> females. At 21 and 28 weeks of age, *Acsbg1*<sup>-/-</sup> mice were ~18% smaller than w.t. mice of the same age (Table 2). Otherwise, the phenotype of *Acsbg1*<sup>-/-</sup> mice was not distinguishable from that of their w.t. littermates. Development, behavior, fertility and lifespan did not appear to be altered by the lack of *Acsbg1*.

**Table 2.** Mouse weights (g ± SEM) at 3 and 4 weeks of age.

	21 Days	n =	21 Days	n =
w.t.	10.0 ± 1.0	9	12.3 ± 1.3	15
<i>Acsbg1</i> <sup>-/-</sup>	8.3 ± 0.5	7	10.1 ± 1.1	12

A unique feature of the strategy used to generate this mouse model is the replacement of *Acsbg1* exon 2 with the  $\beta$ -galactosidase ( $\beta$ -GAL) gene. Thus, tissues that express ACSBG1 in w.t. animals will express  $\beta$ -GAL in KO mice and thus be readily identified. Therefore, we assessed expression of the  $\beta$ -GAL gene in the brain of an *Acsbg1*<sup>-/-</sup> mouse. Sections of brain were fixed in 4% paraformaldehyde and incubated for 2 h in X-gal (5-bromo-4-chloro-3-indolyl- $\beta$ -D-galactosidase) prior to microscopic examination. As seen in Figure 1C,  $\beta$ -galactosidase activity could be detected in cerebral cortical neurons and cerebellar Purkinje cells, known sites of ACSBG1 expression [13]. This result is consistent with  $\beta$ -galactosidase expression being driven by the *Acsbg1* gene promoter.

Previous studies used indirect immunofluorescence (IF) to show that, in addition to cortical neurons and Purkinje cells, ACSBG1 was expressed in cortisol-producing cells of the adrenal gland, testosterone-producing cells of the testis and estrogen-producing cells [13,21]. The lack of ACSBG1 expression in these tissue types in the *Acsbg1*<sup>-/-</sup> mouse was confirmed by Western blotting. ACSBG1 protein was detected in adrenal gland, testis and brain in w.t. mice, but was not seen in *Acsbg1*<sup>-/-</sup> mice (Figure 2). No expression of ACSBG1 was detected in the liver, heart, kidney, lung or spleen in either w.t. or *Acsbg1*<sup>-/-</sup>, as expected (Figure 2).

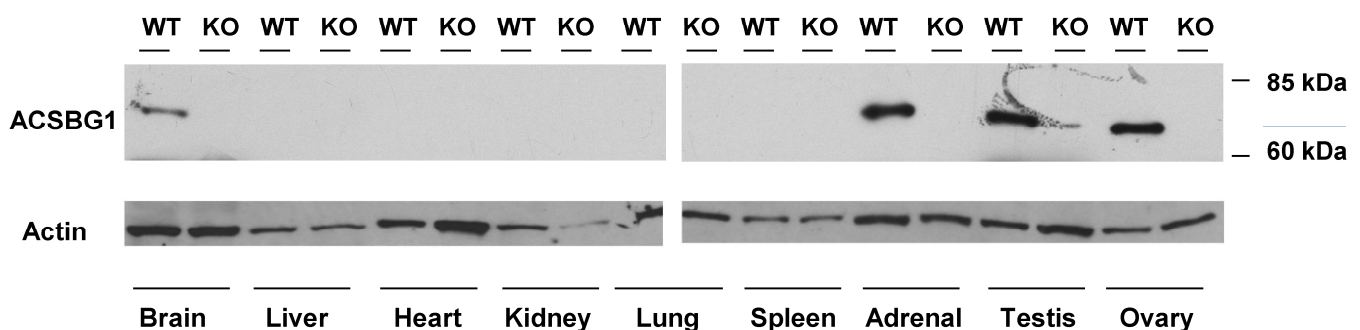


**Figure 2.** Expression of ACSBG1 in mouse tissues. Tissues from adult w.t. and *Acsbg1*<sup>-/-</sup> (KO) mice were homogenized and subjected to Western blot analysis, as described in Materials and Methods. The ~70 kDa ACSBG1 band was observed in brain, adrenal gland, testis and ovary in w.t. mice. GAPDH was used as a loading control.

### 3.2. Acyl-CoA Synthetase Activity in w.t. and *Acsbg1*<sup>-/-</sup> Mouse Tissue

Lack of a specific acyl-CoA synthetase might be expected to lower enzyme activity towards FA known to be substrates in tissue normally expressing the ACS. We previously demonstrated that endogenous ACSBG1 preferred the long-chain FA palmitic acid (C16:0), but only weakly activated the very long-chain FA lignoceric acid (C24:0) [12,14]. Therefore, we prepared tissue homogenates and measured their ability to activate these FA. Because endogenous ACSBG1 in Neuro2a cells sedimented with a mitochondria-enriched fraction [13], we also prepared and assayed ACS activity in brain mitochondria. As shown in Table 3, the lack of ACSBG1 failed to lower C16:0 activation in whole brain, cerebellum, brain mitochondria, adrenal gland or testis. In fact, C16:0 activation in cerebella and adrenal glands of *Acsbg1*<sup>-/-</sup> mice was higher than that measured in w.t. mice. As expected, there was no significant change in ACS activity towards the C24:0 substrate when ACSBG1 was depleted. Similarly, the ACS activity with either substrate was not changed by depletion of ACSBG1 in the liver.

**Table 3.** Tissue ACS activity of w.t. and *Acsbg1*<sup>-/-</sup> mice.

Tissue	C16:0 Activation (nmol/20 min/mg Protein)		C24:0 Activation (nmol/20 min/mg Protein)	
	w.t.	<i>Acsbg1</i> <sup>-/-</sup>	w.t.	<i>Acsbg1</i> <sup>-/-</sup>
Whole brain	16.5	17.3	2.2	2.0
Cerebellum	8.7	16.5	0.6	0.8
Brain mitochondria	26.9	26.7	5.5	5.3
Adrenal gland	38.2	50.0	1.2	1.4
Testis	18.8	18.6	1.7	1.6

Tissue was collected and homogenized in STE. The ability to activate long- or very long-chain FA to their CoA derivatives was measured as described in Materials and Methods, using radiolabeled palmitic acid (C16:0) or lignoceric acid (C24:0), respectively, as substrate.

### 3.3. Regional Distribution of ACSBG1 Expression in Mouse Brain

To determine semi-quantitatively which brain regions normally express ACSBG1, brains from *Acsbg1*<sup>-/-</sup> and w.t. mice were collected and dissected into the cortex, hippocampus, white matter, brainstem and cerebellum. Western blotting revealed that ACSBG1 (~70 kDa band) was expressed in all brain regions in w.t. mice (Figure 3A). Its expression was significantly higher ( $p < 0.01$ ) in the cerebellum than in the other four regions (Figure 3B); cerebellar expression was nearly five-fold higher than that in the cortex. No ACSBG1 protein expression was detectable in any of the *Acsbg1*<sup>-/-</sup> mouse brain regions examined.

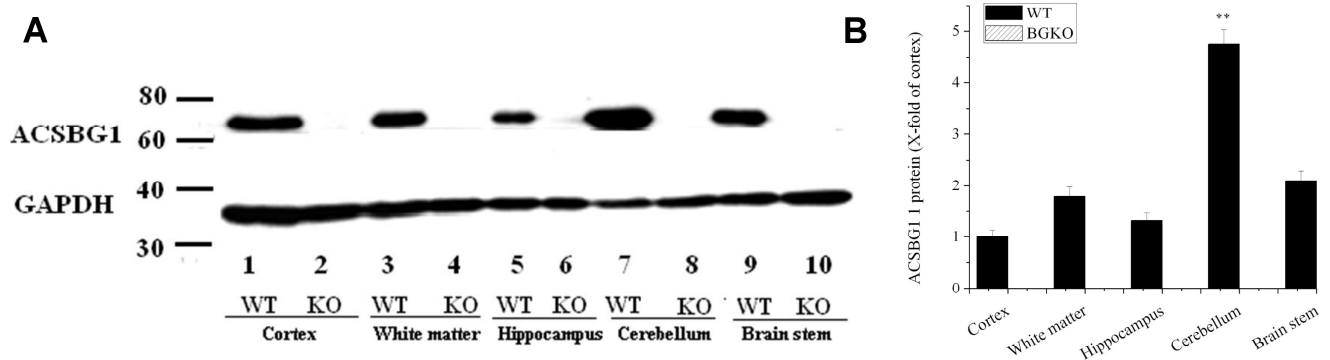


**Figure 3.** Regional expression of ACSBG1 in mouse brain. (A). Western blotting. Brain from adult w.t. and *Acsbg1*<sup>-/-</sup> (KO) was dissected into cortex, hippocampus, white matter, brainstem and cerebellum. Western blotting revealed that ACSBG1 (~70 kDa band) was expressed in all brain regions

in w.t. mice. No ACSBG1 expression was detected in KO mice. GAPDH was used as a loading control. (B). Relative expression of ACSBG1 in brain regions. Densitometry was used to quantify Western blot data. Results were normalized to GAPDH expression and mean  $\pm$  SEM ( $n = 3$ ) was calculated. The fold-increase relative to cortex is shown (\*\*,  $p < 0.01$  relative to cortex).

### 3.4. Brain ACSBG1 Expression Increases with Development of w.t. Mice

The average age of onset of neurological symptoms in CCER is around 6 years, whereas symptoms of AMN typically begin in early adulthood [4]. We therefore wished to determine the developmental expression pattern of ACSBG1 in mouse brain. Since the cerebellum had the highest ACSBG1 expression among the regions examined, we used quantitative PCR and Western blotting to detect *Acsbg1* mRNA and protein levels, respectively, in this area of the brain. In the cerebellum of mice, *Acsbg1* mRNA increased with age and reached a maximum in 1–2-month-old mice (Figure 4A). For ACSBG1 protein expression, there was a very low expression level in 1-, 4- and 8 day-old mice, which increased dramatically with further development and peaked at around 2 months (Figure 4B,  $p < 0.01$  vs. 1 day old). At this age, the *Acsbg1* mRNA level was about five times higher than that found in 1-day-old mice, and the amount of protein expressed was about 100-fold higher. As the mice aged, *Acsbg1* mRNA and protein expression in cerebellum decreased slightly. No *Acsbg1* mRNA or protein was detected in cerebella from *Acsbg1*<sup>-/-</sup> mice at any time point, further confirming the total absence of ACSBG1 in this mouse model.

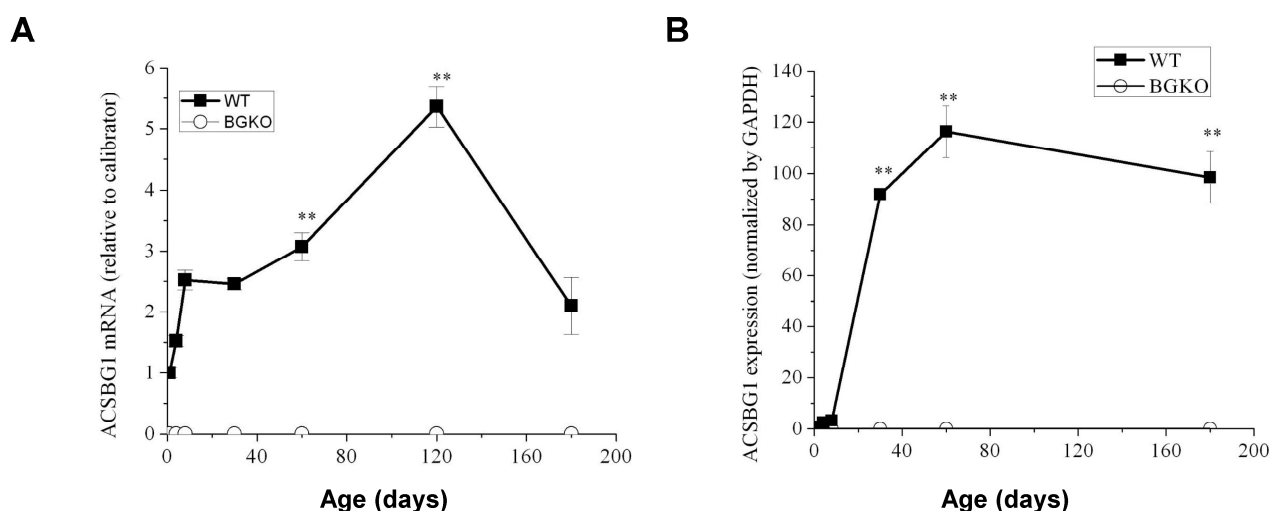


**Figure 4.** Developmental expression of ACSBG1 in cerebellum. (A). mRNA expression. *Acsbg1* mRNA in cerebella from w.t. and *Acsbg1*<sup>-/-</sup> mice of increasing age was measured by quantitative PCR, as described in Materials and Methods. Mean  $\pm$  SEM ( $n = 3$ ) relative to the calibrator is plotted (\*\*,  $p < 0.01$  versus day 1). No *Acsbg1* mRNA was detected in KO mouse cerebellum. (B). Western blotting. ACSBG1 protein expression in cerebella of mice of increasing age was quantitated by densitometric analysis of Western blots. A representative blot is shown in Figure S2. Results were normalized to GAPDH expression. Mean  $\pm$  SEM ( $n = 3$ ) was plotted (\*\*,  $p < 0.01$  relative to day 0). No ACSBG1 protein was detected in KO mouse cerebellum.

### 3.5. ACSBG1 Depletion Decreases Levels of Saturated VLCFA and Monounsaturated FA While Increasing $\omega 3$ Polyunsaturated FA Levels in Cerebella of Adult Mice

The defining biochemical abnormality in XALD is elevated levels of saturated VLCFA [4]. To assess whether the lack of ACSBG1 affected brain FA levels and composition during development, cerebella from w.t. and *Acsbg1*<sup>-/-</sup> mice of different ages were homogenized, their lipids extracted and the FA composition measured by GC/MS, as described in Materials and Methods. We first looked at the differences between classes of fatty acids, e.g., saturated,  $\omega 9$  monounsaturated and  $\omega 6$  polyunsaturated, in w.t. and *Acsbg1*<sup>-/-</sup> mice. As shown in Table 4 and Figure S3, total saturated FA (C10-30, which constitute nearly half



of total FA) were mainly unchanged with age but tended to be slightly lower in *Acsbg1*<sup>-/-</sup> mice. When we looked only at VLCFA (C22-30; ~3% of total FA in adult mice), we found that the levels of these FA were barely detectable at birth and increased relatively linearly over the first 50 days of life. The levels in *Acsbg1*<sup>-/-</sup> cerebella were lower than in w.t. mice. From 50 to 180 days, the saturated VLCFA slightly increased in w.t. mice, while remaining the same or decreasing somewhat in *Acsbg1*<sup>-/-</sup> mice. The lower VLCFA in ACSBG1-deficient mice is thus in contrast to the increased VLCFA seen in XALD mice.

**Table 4.** Changes in cerebellar FA levels in w.t. and *Acsbg1*<sup>-/-</sup> mice with age.

Age (Days)		1	4	8	15	50	120	180
Total saturated FA	w.t.	47.5	48.6	47.0	47.3	46.4	45.9	44.9
	<i>Acsbg1</i> <sup>-/-</sup>	40.4	47.2	47.1	47.0	45.3	46.7	43.4
Total sat. VLCFA (C22-30)	w.t.	0.2	0.2	0.3	1.2	2.7	2.8	3.2
	<i>Acsbg1</i> <sup>-/-</sup>	0.1	0.2	0.4	1.0	2.5	2.3	2.4
Total ω9 FA	w.t.	14.9	13.8	14.2	15.9	21.3	21.7	24.2
	<i>Acsbg1</i> <sup>-/-</sup>	15.3	13.6	13.8	14.6	19.0	20.3	21.0
Total ω5+ω7 FA	w.t.	5.4	4.9	5.2	4.3	4.3	4.1	4.4
	<i>Acsbg1</i> <sup>-/-</sup>	5.2	5.3	4.9	4.4	4.6	4.2	4.8
Total ω6 FA	w.t.	17.8	18.5	18.7	18.0	12.5	12.4	11.8
	<i>Acsbg1</i> <sup>-/-</sup>	21.2	18.0	19.0	18.8	13.5	13.0	12.8
Total ω3 FA	w.t.	11.6	11.7	12.7	13.6	15.3	15.7	14.7
	<i>Acsbg1</i> <sup>-/-</sup>	15.0	13.4	13.2	14.0	17.6	16.7	18.1
Total trans FA	w.t.	2.9	2.6	2.2	0.9	0.2	0.2	0.2
	<i>Acsbg1</i> <sup>-/-</sup>	2.9	2.7	2.1	1.2	0.1	0.2	0.1

Cerebellum was collected from w.t. and *Acsbg1*<sup>-/-</sup> mice at 1, 4, 8, 15, 50, 120 and 180 days of age. Lipids were extracted and total lipid FA were quantitated as described in Materials and Methods. Levels of FA in different classes are shown as percentage of total FA. These data are also shown graphically in Figure S3.

In both w.t. and *Acsbg1*<sup>-/-</sup> mice, total ω9 monounsaturated FA (constituting ~20% of total FA in adult mice) increased slightly over the first 50 days of life and then remained relatively constant up to 180 days. At every time point, the levels were somewhat higher in w.t. than in *Acsbg1*<sup>-/-</sup> cerebella. Levels of ω5 + ω7 monounsaturated FA (~5% of total FA) decreased over the first fifteen days of life and then remained relatively constant; at all ages levels were similar in both groups of mice. The ω6 polyunsaturated FA (~12% of total FA in adults) decreased over the first 50 days of life, before remaining constant thereafter; the levels of these FA were consistently slightly higher in ACSBG1-deficient mice. Interestingly, the levels of ω3 polyunsaturated FA (~15% of total FA in adults) were also consistently higher in knockout mice relative to w.t. animals; levels rose slightly over the first 50 days of life and did not change appreciably thereafter. The total trans-FA decreased from about 3% of total FA to nearly zero over the first 50 days and were barely detectable thereafter; levels in w.t. and ACSBG1-deficient cerebella were not different.

### 3.6. Levels of Specific FA Are Affected by ACSBG1 Depletion in Cerebella of Adult Mice

Not all FA of a specific class, e.g., monounsaturated FA, were affected by the lack of ACSBG1. In Figure 5, the age-related changes in the levels of several FA are shown. Some are typical members of a given class, while others are specific members that show changes in *Acsbg1*<sup>-/-</sup> mice. Levels of the two most abundant saturated FA in nature—C16:0 (palmitic acid) and C18:0 (stearic acid)—were unchanged by ACSBG1 knockout. In contrast, the levels of saturated very long-chain FA containing 24 (lignoceric acid) and 26 carbons (cerotic acid) were significantly lower in *Acsbg1*<sup>-/-</sup> mice. Among the ω9

monounsaturated FA, the levels of both the abundant C18:1 (oleic acid) and the very long-chain C24:1 (nervonic acid) were lower in cerebella of *Acsbg1*<sup>-/-</sup> mice. Interestingly, both saturated and monounsaturated VLCFA increased from nearly zero at birth to steady-state levels at around 2 months of age. In contrast, the levels of both C16:1 $\omega$ 9 and C16:1 $\omega$ 7 monounsaturates decreased from more than 2% of total FA at birth to very low ( $\omega$ 7) and nearly undetectable ( $\omega$ 9) levels at 2 months of age; there were no differences between w.t. and *Acsbg1*<sup>-/-</sup> mice.

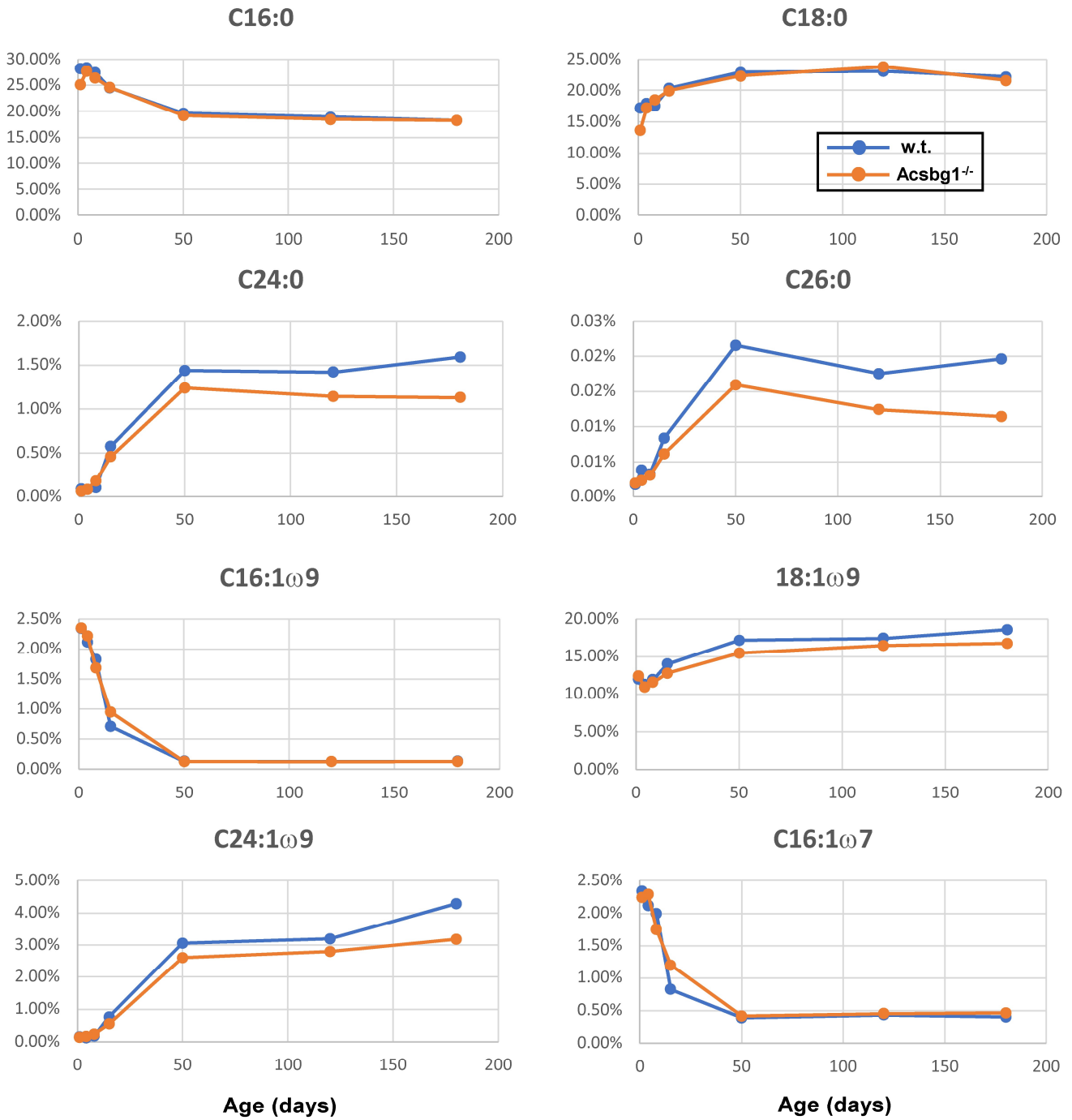
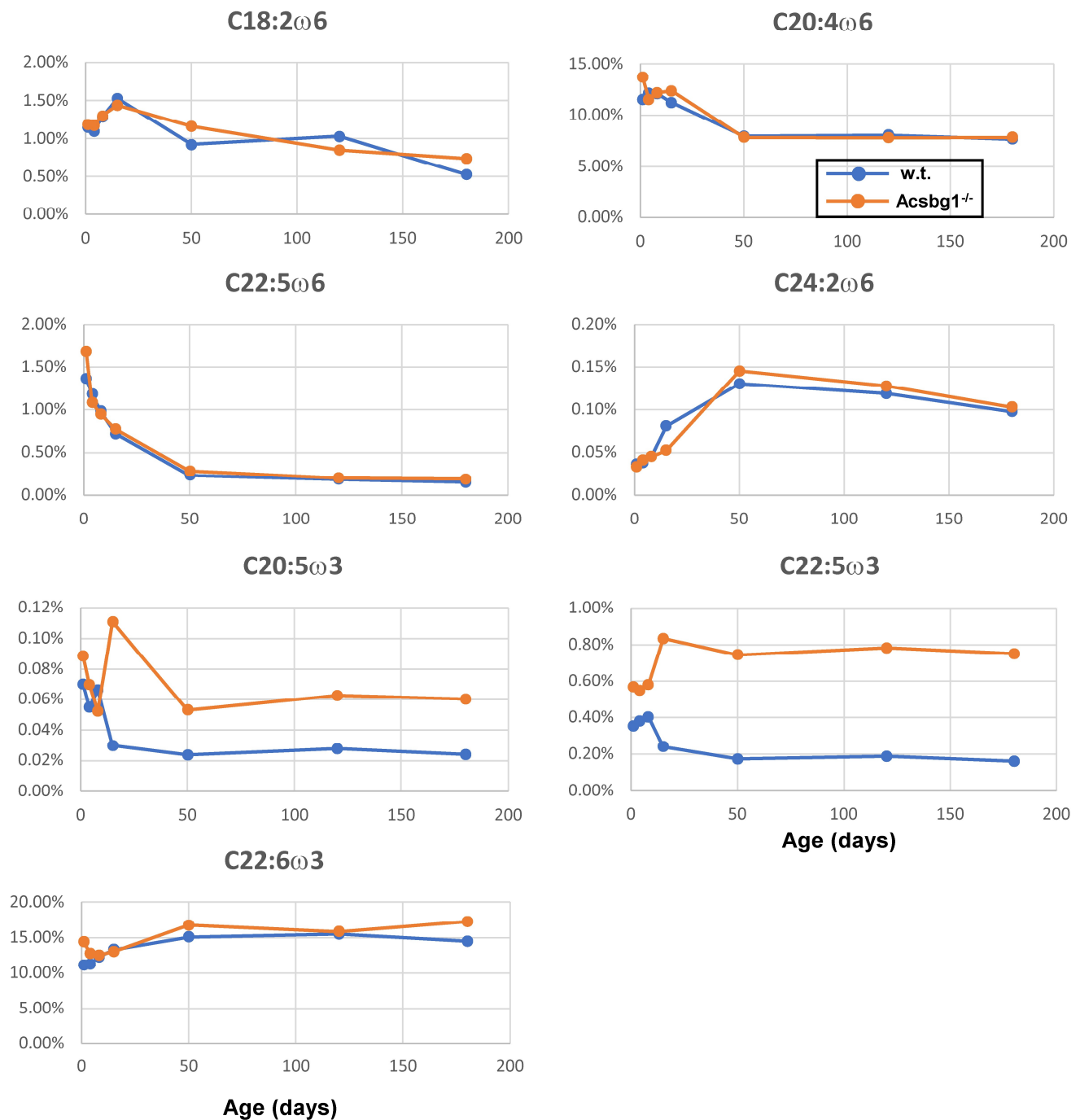


Figure 5. Cont.



**Figure 5.** Changes with age in levels of specific cerebellar FA in w.t. and *Acsbg1*<sup>-/-</sup> mice. Lipids were extracted from cerebellum and levels of specific FA quantitated as described in the legend to Table 4. Levels of specific FA as percentage of total FA are shown. (—○—, w.t.; —○—, *Acsbg1*<sup>-/-</sup>).

Among the  $\omega$ 6 polyunsaturated FA, none showed a significant difference in level between w.t. and *Acsbg1*<sup>-/-</sup> mice. There were, however, some age-related changes. Plots of FA level vs. age are shown for C18:2 (linoleic acid), C20:4 (arachidonic acid), C22:5 (docosapentaenoic acid) and C24:2.

The lack of ACSBG1 did produce changes in levels of some, but not all, polyunsaturated FA of the  $\omega$ 3 series. Specifically, levels of C20:5 (eicosapentaenoic acid) and C22:5 were significantly higher in *Acsbg1*<sup>-/-</sup> mice.

### 3.7. Depletion of ACSBG1 Affects the Developmental Expression Pattern of Enzymes Required for De Novo FA Synthesis in Mouse Cerebellum

Differences in the FA profile of cerebella from w.t. and *Acsbg1*<sup>-/-</sup> mice (Table 4, Figures 5 and S3) suggest that the presence or absence of ACSBG1 has effects on lipid metabolism during mouse brain development. To understand better the role of ACSBG1 in these processes in the cerebellum, we quantified several enzymes relevant to FA synthesis and degradation by qRT-PCR and Western blotting in w.t. and *Acsbg1*<sup>-/-</sup> mice. Acetyl-CoA carboxylase 1 (ACC1) catalyzes the regulated initial step in de novo FA synthesis—the carboxylation of acetyl-CoA to form malonyl-CoA [22]. As shown in Figure 6A, *ACC1* mRNA in the cerebella of w.t. mice decreased during the first month of life (days 1–30) and then slowly increased over the next 5 months (days 30–180). In ACSBG1-deficient mice, *ACC1* mRNA was significantly higher than in w.t. mice in the early postnatal period, but, by 8–15 days of age, the levels were similar. However, while *ACC1* expression slowly rebounded in w.t. mice, the mRNA levels continued to decline in *Acsbg1*<sup>-/-</sup> mice so that, by 4–6 months of age (days 120–180), the mRNA levels were significantly lower in *Acsbg1*<sup>-/-</sup> mice than in w.t. mice. In addition to mRNA, we also measured ACC1 protein expression by densitometric scanning of Western blots. In general, ACC1 protein quantitation in w.t. and *Acsbg1*<sup>-/-</sup> mice paralleled that of the *Acc1* mRNA levels (Figure 6B). The time-dependent decrease in ACC1 protein level was more linear than what was seen with mRNA levels, and the drop in ACSBG1-deficient mouse cerebellum was more acute than in w.t. (Figure 6C). Fatty acid synthase (FASN) is a large multienzyme complex whose component domains catalyze all reactions of de novo FA synthesis downstream of ACC1 [23]. Like ACC1, cerebellar *Fasn* mRNA was high in the early postnatal period of w.t. mice and decreased to a low, steady state by 2–4 months of age (days 60–120); Figure 6D). In *Acsbg1*<sup>-/-</sup> mice, mRNA levels also started high but decreased slightly more rapidly than in w.t. mice; at 6 months (180 days) of age *Fasn* mRNA levels were lower in *Acsbg1*<sup>-/-</sup> mice. FASN protein expression in general paralleled mRNA expression in both w.t. and *Acsbg1*<sup>-/-</sup> mice (Figure 6E).

### 3.8. mRNA Expression of Several Other FA Metabolism Enzymes Is Affected by ACSBG1 Deficiency

We measured the mRNA expression of several additional enzymes involved in FA metabolism in cerebella from w.t. and *Acsbg1*<sup>-/-</sup> mice. While ACC1 is essential for de novo FA synthesis in lipogenic tissues, its isoform ACC2 produces malonyl-CoA primarily to regulate FA degradation via the inhibition of carnitine palmitoyltransferase 1 (CPT1) and carnitine octanoyltransferase (CROT) in mitochondria and peroxisomes, respectively [22,24]. *Acc2* mRNA levels were quantitated by RT-PCR in cerebella from w.t. and *Acsbg1*<sup>-/-</sup> mice (Figure 7A). In general, there was no major change during mouse development and no significant difference between w.t. and *Acsbg1*<sup>-/-</sup> mice, except for dramatic reductions in *ACC2* expression in *Acsbg1*<sup>-/-</sup> mice on days 1, 15 and 180.

FA desaturases FADS1 and FADS2 participate in the synthesis of polyunsaturated FA by the insertion of double bonds with five or six carbons (respectively) from the carboxyl carbon [25]. The mRNA levels of both desaturases decreased with increasing age of w.t. mice, reaching a relative steady state by around one month of age (day 30) (Figure 7B,C). The steady-state level of *Fads2* mRNA, however, was significantly lower than that seen with *Fads1* mRNA.

FA elongases (ELOVL family) catalyze the initial step in adding two-carbon units to long-chain FA to produce very long-chain FA [26]. In particular, ELOVL2 and ELOVL5 work in concert with the desaturases to produce polyunsaturated FA of increasing chain lengths [26]. The *Elovl2* mRNA levels in w.t. mice were high at birth but rapidly decreased to a rather steady-state level by 2 weeks of age (Figure 7D). In *Acsbg1*<sup>-/-</sup> mice, the mRNA levels were lower than in w.t. at birth and did not change appreciably throughout life. On the other hand, the levels of *Elovl5* mRNA in the cerebellum from w.t. mice were low at birth, but increased and reached a relative steady state by about day 15 (Figure 7E). In

*Acsbg1*<sup>-/-</sup> mice, the *Elovl5* mRNA levels were significantly higher at birth and remained rather constant throughout life. However, in 120–180-day-old mice, mRNA levels were higher in w.t. than in *Acsbg1*<sup>-/-</sup> mice.

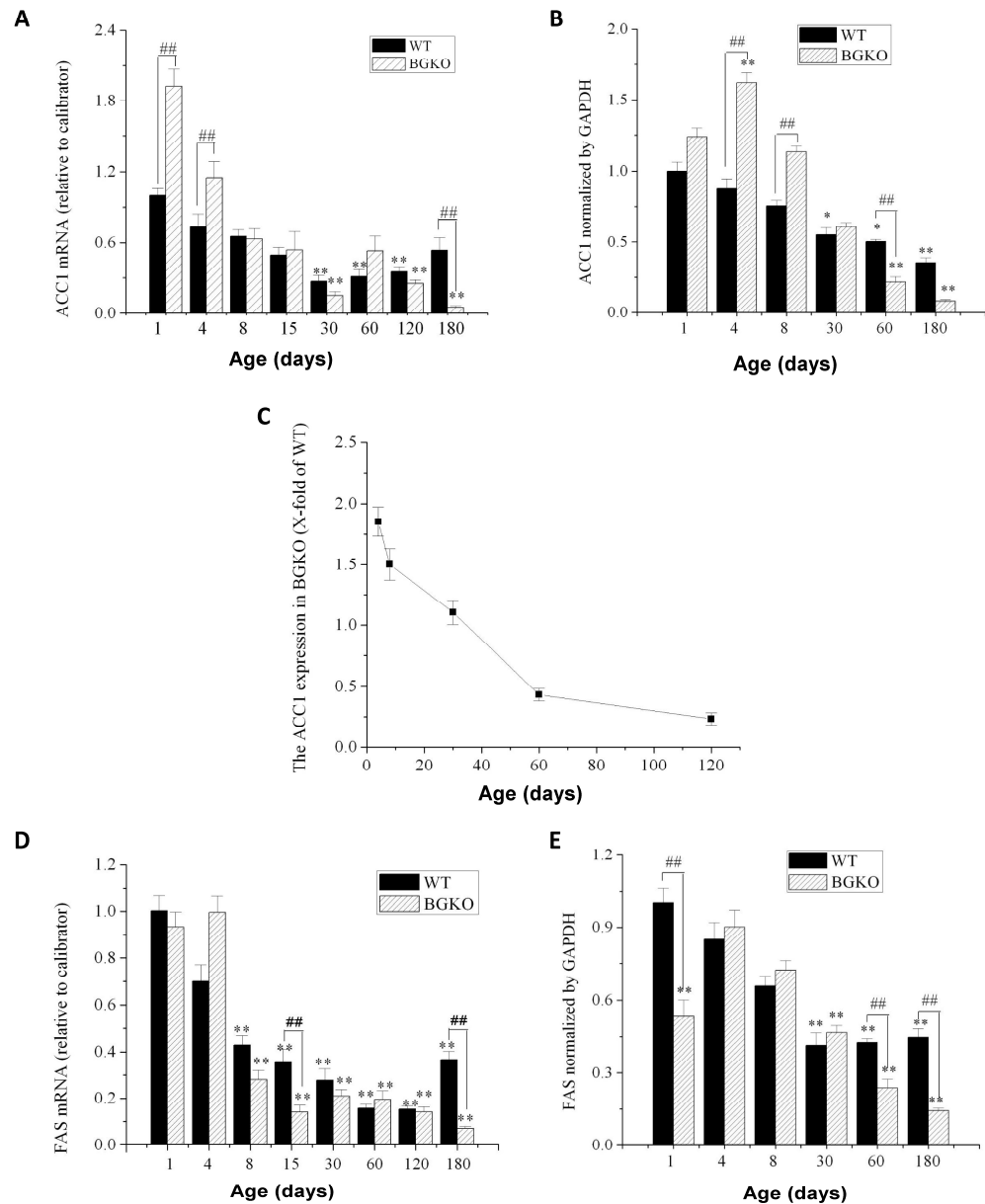


**Figure 6.** Developmental expression of de novo FA synthesis enzymes in cerebellum from w.t. and *Acsbg1*<sup>-/-</sup> mice. Cerebella were obtained from w.t. and *Acsbg1*<sup>-/-</sup> mice at several time points from day 1 to day 180 of age, and the expression of FA synthesis enzyme mRNA and protein was measured. For all studies, the mean ± SEM (n = 3) is plotted. (A) *ACC1* mRNA level measured by quantitative PCR and (B) protein expression of *ACC1* quantitated by Western blotting in cerebella of w.t. and *Acsbg1*<sup>-/-</sup> mice at the indicated age. (C) is a derivative plot of the data shown in panel B, created by dividing KO mouse expression by w.t. expression. (D) *FASN* mRNA level measured by quantitative PCR and (E) protein expression of *FASN* quantitated by Western blotting in cerebella of w.t. and *Acsbg1*<sup>-/-</sup> mice at the indicated age. The significance of differences in expression relative to that in 1-day-old w.t. mice is indicated by asterisks (\*, *p* < 0.05, \*\*, *p* < 0.01). Hashtags (##) indicate the significance of the differences in w.t. versus *Acsbg1*<sup>-/-</sup> mice on a given day (##, *p* < 0.01). Densitometry of ~70 kDa ACSBG1 bands on Western blots was normalized to GAPDH.

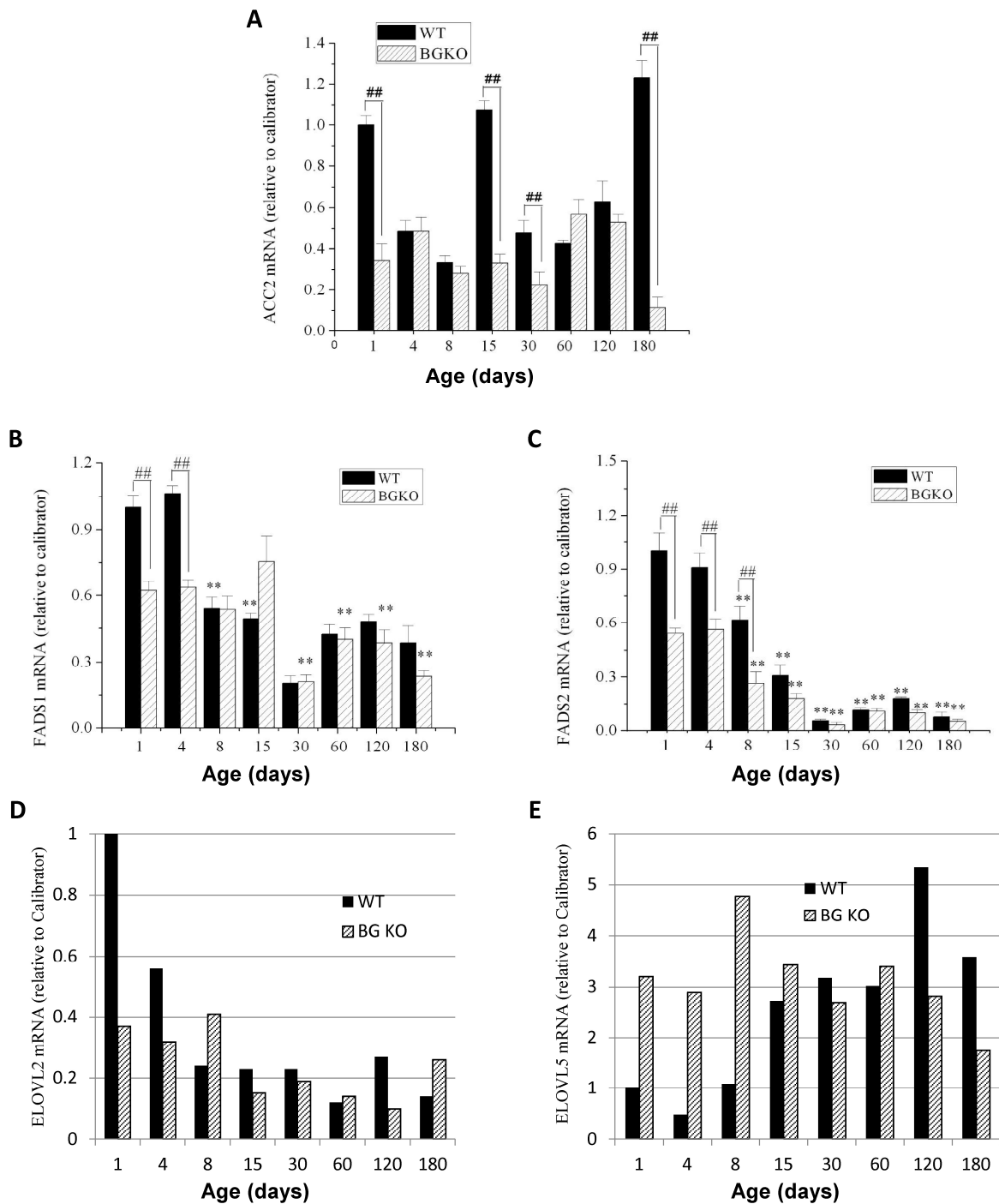


**Figure 7.** Developmental expression of enzymes participating in FA degradation, elongation and unsaturation in cerebella from w.t. and *Acsbg*<sup>-/-</sup> mice. Quantitative PCR was used to measure the mRNA levels of several additional FA metabolism enzymes, including (A) ACC2, a regulator of fatty acid entry into mitochondria for degradation by  $\beta$ -oxidation; (B) FADS1 and (C) FADS2, desaturases relevant to the synthesis of  $\omega$ 3 polyunsaturated FA; and (D) ELOVL2 and (E) ELOVL5, elongases that are also relevant to  $\omega$ 3 polyunsaturated FA synthesis. In panels (A–C), triplicate analyses were done and the significance of the differences in expression relative to that in 1-day-old w.t. mice is indicated by asterisks (\*\*,  $p < 0.01$ ). The significance of expression differences in w.t versus *Acsbg*<sup>-/-</sup> mice on a given day is indicated by hashtags (##,  $p < 0.01$ ). For panels (D,E), only duplicate analyses were performed.

#### 4. Discussion

Amongst the inherited metabolic diseases, XALD is one of the most prevalent, with an allele frequency of about 1 in 17,000 [27]. Nearly all male patients have some degree of adrenal gland insufficiency. While some will develop central demyelination in childhood, namely the CCER XALD phenotype, most will manifest symptoms of peripheral nervous system disease, namely adrenomyeloneuropathy (AMN), in early adulthood [4]. Progression to the CCER phenotype in later adulthood is seen in more than 50% of AMN patients [28]. In addition, some AMN patients show signs of testicular involvement, including decreased spermatogenesis or infertility [4]. Thus, the pathology in XALD is limited to a relatively small number of tissue types. In contrast, *ABCD1*, the gene that is defective in XALD, has a rather ubiquitous tissue expression profile (Figure S1). *ABCD1* expression is highest in adipose tissue and small intestine—tissue types that have not been shown to be clinically affected in XALD. While the testis and adrenal gland have the next highest *ABCD1* expression, the levels of brain *ABCD1* are among the lowest found in human tissue. Why, therefore, is the pathology in XALD limited to only a few tissue types?

A definitive explanation for this remains elusive. One hypothesis is that the involved tissues have unique metabolic features that render them more vulnerable to the high levels of VLCFA that are the biochemical signature of XALD [29,30]. Several properties of ACSBG1, identified in a screen of fruit fly neurodegeneration mutants [3], suggested that exploration of its potential role in XALD pathogenesis was warranted. When first discovered, ACSBG1 was a previously unknown member of the ACS enzyme family. ACSs occupy a central position in lipid metabolism by activating FA to their CoA derivatives, a necessary prerequisite for subsequent participation in either catabolic or anabolic processes [1]. In addition to neurodegeneration, ACSBG1-deficient flies had elevated tissue levels of VLCFA, similar to the situation in XALD patients [4]. We and others found that, in humans and mice, expression of ACSBG1 was primarily in the tissue types pathologically affected in XALD, namely the brain, adrenals and testis [13,14]. These observations prompted us to create a knockout mouse model to test the relationship between ACSBG1 and XALD.

The *Acsbg1*<sup>-/-</sup> mouse described herein was generated by the replacement of exon 2 with a  $\beta$ -GAL gene. Sheng et al. [31] created a similar knockout mouse by deletion of a ~2 kb fragment of the *Acsbg1* gene that included the start codon; these researchers originally called this gene “gonadotropin-regulated long chain fatty acid Acyl-CoA synthetase” (*GR-LACS*). No gross phenotypic abnormalities were observed in either our *Acsbg1*<sup>-/-</sup> mouse or the *GR-LACS*<sup>-/-</sup> mouse. Studies of *Acsbg1*<sup>-/-</sup> mice from both laboratories confirmed that the tissue types expressing ACSBG1 were identical to those pathologically affected in XALD. We did observe a mild growth phenotype that was not present in the *GR-LACS*<sup>-/-</sup> mouse.

The lack of ACSBG1 did not reduce ACS activity with either C16:0 or C24:0 as substrate in tissues from *Acsbg1*<sup>-/-</sup> mice produced by either laboratory, suggesting that there was compensatory upregulation of other ACS genes. Preliminary studies suggest that two members of the ACSVL (SLC27A) family are indeed slightly upregulated (SLC27A1, SLC27A4), while others (SLC27A2, SLC27A3) are somewhat downregulated (Y Li, unpublished observation). Additional experiments to assess the effect of *Acsbg1* deficiency on the expression of other ACS enzymes, particularly members of the ACSL family, will be conducted to clarify this issue. In the future, lipidomic analyses may also shed light on the specific lipids that are altered when ACSBG1 is deficient.

When we looked at the relative expression of ACSBG1 in various brain regions, we observed that the highest expression was in the cerebellum (Figure 3). To probe further the potential relevance of ACSBG1 in XALD, we looked at the expression of this protein during brain development. We found ACSBG1 to be very low at birth and throughout the first few days of life, after which there was a robust increase in expression (Figure 4). In contrast, the expression of *ABCD1* was reported to be at its highest from embryonic day 12 through postnatal day 15, after which its expression dropped 2.6-fold by adulthood [32]. Thus, there was little correlation between expression of the two proteins with age.

Because *Drosophila* “bubblegum” mutants had elevated levels of saturated VLCFA [3], similar to XALD patients [4], we expected that *Acsbg1*<sup>−/−</sup> mice would also exhibit a similar elevation, particularly in the brain. While cerebellar total saturated FA levels in w.t. and *Acsbg1*<sup>−/−</sup> mice were essentially the same from birth to 6 months of age, the VLCFA levels differed. However, instead of the predicted increase in VLCFA levels in *Acsbg1*<sup>−/−</sup> mouse cerebellum, saturated VLCFA levels were consistently lower (Table 4 and Figure S3). This observation decreases the likelihood that ACSBG1 has a direct role in XALD pathophysiology. Interestingly, a pattern similar to cerebellar VLCFA levels in w.t. vs. *Acsbg1*<sup>−/−</sup> mice was seen for total ω9 monounsaturated FA, and the reverse was detected for total polyunsaturated ω3 FA, where the levels in *Acsbg1*<sup>−/−</sup> mice were higher than in w.t.

When we looked at individual cerebellar FA levels in w.t. and *Acsbg1*<sup>−/−</sup> mice from birth to 6 months of age (Figure 5), a few comparisons were notable. Since C16:0 (palmitic acid) is a preferred substrate for ACSBG1 [12,14], it was predicted that the levels of this FA would be lower in tissues from *Acsbg1*<sup>−/−</sup> mice. However, essentially no differences between w.t. and *Acsbg1*<sup>−/−</sup> mouse C16:0 content were noted throughout the first 6 months of life. A similar pattern was seen with C18:0 (stearic acid). In contrast, by two months of age, the levels of saturated VLCFA C24:0 and C26:0 were clearly lower in *Acsbg1*<sup>−/−</sup> mouse cerebellum, and this gap grew wider with age to at least 6 months. A similar pattern was seen with the ω9 monounsaturated VLCFA C24:1 (nervonic acid) and, to a lesser extent, with C18:1ω9 (oleic acid).

The increase in total ω3 polyunsaturated FA noted above was primarily due to increases in C22:6ω3 (docosahexaenoic acid; DHA). Brain and cerebellar DHA levels are surprisingly high, accounting for up to 25% of total brain FA in humans [33]. Although C20:5ω3 (eicosapentaenoic acid; EPA) and C22:5ω3 (docosapentaenoic acid; DPA) are intermediates in the synthesis of DHA [34], it seems unlikely that the increased EPA and DPA contribute significantly here, as the levels of these FA are about three and two orders of magnitude lower (respectively) than those of DHA. A large number of previous studies have indicated that ω3 polyunsaturated FA are essential for normal growth and development. The health effects of these FAs include a reduction in cardiovascular risk due to antiarrhythmic, anti-inflammatory, anti-thrombotic and lipid-lowering actions, as well as improved glucose level control and insulin sensitivity and neuroprotection [34–37]. Thus, reduced ACSBG1 expression could be associated with improvements in cardiovascular disease, reduced complications of diabetes and a lowered risk for depression. These effects could be mediated by eicosanoids and/or docosanoids derived from these ω3 polyunsaturated FA, where even very low levels of signaling molecules can have highly significant biological activity. The effects of increased polyunsaturated ω3 FA could also be mediated by changes in membrane fluidity. These changes can alter the structure of microdomains (lipid rafts) that are thought to serve as signaling platforms in cell membranes [38]. Further investigation into the effect of ACSBG1 depletion on eicosanoid- and docosanoid-mediated signaling in the brain is clearly warranted.

Sheng et al. also measured the FA levels in adult brain, testis, ovary and adrenal gland in their *Acsbg1*<sup>−/−</sup> mouse [31]. Our findings in the cerebellum and their findings in the whole brain are in general agreement for many FA, including C16:0, C18:1, C24:1, C20:5ω3, C22:5ω3 and C22:6ω3.

The long-chain saturated FA palmitate (C16:0) is produced by the de novo FA synthesis pathway that includes acetyl-CoA carboxylase (ACC1) and fatty acid synthase (FASN) [22,23]. C16:0 can then be elongated to produce VLCFA. At and shortly after birth, cerebella from *Acsbg1*<sup>−/−</sup> mice had higher levels of both ACC1 and FASN (Figure 6) than did w.t. mice, indicating a potentially higher capacity to synthesize C16:0 by *Acsbg1*<sup>−/−</sup> mice. The expression of these enzymes dropped with increasing age in both w.t. and *Acsbg1*<sup>−/−</sup> mice. This was particularly evident when the ratio of *Acsbg1*<sup>−/−</sup> to w.t. ACC1 was plotted (Figure 6C), and possibly contributes to the lower VLCFA levels measured in knockout mouse cerebellum. In contrast to ACC1, the malonyl-CoA product of ACC2



is used primarily to regulate FA degradation by the mitochondrial  $\beta$ -oxidation pathway. *ACC2* expression levels, shown in Figure 7A, did not suggest a significant effect of ACSBG1 deficiency on FA oxidation.

Unlike saturated VLCFA, which can be produced by de novo synthesis and subsequent elongation,  $\omega$ 3 and  $\omega$ 6 FA are “essential”, meaning that at least some of these must originate from the diet. However, once ingested, most essential FA can be interconverted [25,35,39]. Interconversion enzymes include desaturases and elongases. Other than in the first few days of life, the expression levels of desaturases *FADS1* and *FADS2* were essentially the same in both w.t. and *Acsbg1*<sup>-/-</sup> mice. Expression of *ELOVL2* was generally not higher in *Acsbg1*<sup>-/-</sup> mice than in w.t. mice and therefore cannot easily explain the higher levels of C20:5 $\omega$ 3 and C22:5 $\omega$ 3 in *Acsbg1*<sup>-/-</sup> mice. During the first week of life, *ELOVL5* was higher in *Acsbg1*<sup>-/-</sup> mice than in w.t. but, thereafter, was the same or lower; this is, again, in contrast to the elevated C20:5 $\omega$ 3 and C22:5 $\omega$ 3 levels. *ELOVL1* must be evaluated in future studies, as this enzyme is also required for some interconversion steps in  $\omega$ 3 FA synthesis.

The results of these studies confirm that, despite appealing circumstantial evidence, ACSBG1 does not play a central role in XALD pathophysiology and is thus not a therapeutic target in XALD. The findings published by Sheng et al. [31] indicate that the absence of ACSBG1 affects testicular Leydig cell function, but any effect(s) on the brain, adrenal gland and ovary remain elusive. Several parameters of cerebellar lipid metabolism are clearly affected when ACSBG1 is defective. Further investigation is needed to clarify these and other roles of ACSBG1 in metabolism.

Metabolic function becomes specialized as development progresses, adapting to tissue-specific needs. Despite its potential role in XALD, the exact function of ACSBG1 remains unclear. Our studies using *Acsbg1*<sup>-/-</sup> mice have revealed unexpected findings, particularly regarding the levels of saturated VLCFA in the cerebellum. Contrary to expectations, VLCFA levels were consistently lower in *Acsbg1*<sup>-/-</sup> mice, challenging the direct involvement of ACSBG1 in XALD pathology. However, the intriguing patterns in monounsaturated and polyunsaturated fatty acids suggest a complex role for ACSBG1 in lipid metabolism and associated disorders. Further research is needed to fully elucidate the function of ACSBG1 and its implications in metabolic diseases.

**Supplementary Materials:** The following supporting information can be downloaded at: <https://www.mdpi.com/article/10.3390/cells13201687/s1>, Figure S1. Relative expression of *ABCD1* mRNA in tissues. Figure S2. ACSBG1 protein expression in developing mouse cerebellum. Figure S3. Changes with age in different classes of cerebellar FA in w.t. and *Acsbg1*<sup>-/-</sup> mice.

**Author Contributions:** Conceptualization, K.D.S., Y.L. and P.A.W.; experimentation, Y.L., X.Y., D.G.-L., Z.P. and A.B.M.; writing, X.Y. and P.A.W.; review and editing X.Y., Y.L., D.G.-L., Z.P., A.B.M., K.D.S. and P.A.W. All authors have read and agreed to the published version of the manuscript.

**Funding:** This work was supported by NIH grants NS37355, HD10981 and HD24061.

**Institutional Review Board Statement:** The Johns Hopkins University School of Medicine Institutional Animal Care and Use Committee (IACUC)MO05M413 (Kirby Smith)/MO09M59 (Paul Watkins).

**Informed Consent Statement:** Not applicable.

**Data Availability Statement:** The raw data supporting the conclusions of this article will be made available by the authors on request.

**Conflicts of Interest:** The authors declare no conflicts of interest.

## References

1. Watkins, P.A. Fatty acid activation. *Prog. Lipid Res.* **1997**, *36*, 55–83. [CrossRef] [PubMed]
2. Watkins, P.A.; Maignel, D.; Jia, Z.; Pevsner, J. Evidence for 26 distinct acyl-coenzyme A synthetase genes in the human genome. *J. Lipid Res.* **2007**, *48*, 2736–2750. [CrossRef] [PubMed]
3. Min, K.T.; Benzer, S. Preventing neurodegeneration in the *Drosophila* mutant bubblegum. *Science* **1999**, *284*, 1985–1988. [CrossRef] [PubMed]

4. Moser, H.W.; Smith, K.D.; Watkins, P.A.; Powers, J.; Moser, A.B. X-linked Adrenoleukodystrophy. In *The Metabolic and Molecular Bases of Inherited Disease*, 8th ed.; Scriver, C.R., Beaudet, A.L., Sly, W.S., Valle, D., Eds.; McGraw-Hill: New York, NY, USA, 2001; pp. 3257–3301.
5. Lazo, O.; Contreras, M.; Hashmi, M.; Stanley, W.; Irazu, C.; Singh, I. Peroxisomal lignoceroyl-CoA ligase deficiency in childhood adrenoleukodystrophy and adrenomyeloneuropathy. *Proc. Natl. Acad. Sci. USA* **1988**, *85*, 7647–7651. [[CrossRef](#)] [[PubMed](#)] [[PubMed Central](#)]
6. Wanders, R.J.; van Roermund, C.W.; van Wijland, M.J.; Schutgens, R.B.; van den Bosch, H.; Schram, A.W.; Tager, J.M. Direct demonstration that the deficient oxidation of very long chain fatty acids in X-linked adrenoleukodystrophy is due to an impaired ability of peroxisomes to activate very long chain fatty acids. *Biochem. Biophys. Res. Commun.* **1988**, *153*, 618–624. [[CrossRef](#)] [[PubMed](#)]
7. Mosser, J.; Douar, A.M.; Sarde, C.O.; Kioschis, P.; Feil, R.; Moser, H.; Poustka, A.M.; Mandel, J.L.; Aubourg, P. Putative X-linked adrenoleukodystrophy gene shares unexpected homology with ABC transporters. *Nature* **1993**, *361*, 726–730. [[CrossRef](#)] [[PubMed](#)]
8. Braiterman, L.T.; Zheng, S.; Watkins, P.A.; Geraghty, M.T.; Johnson, G.; McGuinness, M.C.; Moser, A.B.; Smith, K.D. Suppression of peroxisomal membrane protein defects by peroxisomal ATP binding cassette (ABC) proteins. *Hum. Mol. Genet.* **1998**, *7*, 239–247. [[CrossRef](#)] [[PubMed](#)]
9. Wiesinger, C.; Kunze, M.; Regelsberger, G.; Forss-Petter, S.; Berger, J. Impaired very long-chain acyl-CoA  $\beta$ -oxidation in human X-linked adrenoleukodystrophy fibroblasts is a direct consequence of ABCD1 transporter dysfunction. *J. Biol. Chem.* **2013**, *288*, 19269–19279. [[CrossRef](#)] [[PubMed](#)] [[PubMed Central](#)]
10. Morita, M.; Shimozawa, N.; Kashiwayama, Y.; Suzuki, Y.; Imanaka, T. ABC subfamily D proteins and very long chain fatty acid metabolism as novel targets in adrenoleukodystrophy. *Curr. Drug Targets* **2011**, *12*, 694–706. [[CrossRef](#)] [[PubMed](#)]
11. van Roermund, C.W.; Visser, W.F.; Ijlst, L.; van Cruchten, A.; Boek, M.; Kulik, W.; Waterham, H.R.; Wanders, R.J. The human peroxisomal ABC half transporter ALDP functions as a homodimer and accepts acyl-CoA esters. *FASEB J.* **2008**, *22*, 4201–4208. [[CrossRef](#)] [[PubMed](#)]
12. Steinberg, S.J.; Morgenthaler, J.; Heinzer, A.K.; Smith, K.D.; Watkins, P.A. Very long-chain acyl-CoA synthetases. Human “bubblegum” represents a new family of proteins capable of activating very long-chain fatty acids. *J. Biol. Chem.* **2000**, *275*, 35162–35169. [[CrossRef](#)] [[PubMed](#)]
13. Pei, Z.; Oey, N.A.; Zuidervaart, M.M.; Jia, Z.; Li, Y.; Steinberg, S.J.; Smith, K.D.; Watkins, P.A. The acyl-CoA synthetase “bubblegum” (lipidosin): Further characterization and role in neuronal fatty acid beta-oxidation. *J. Biol. Chem.* **2003**, *278*, 47070–47078. [[CrossRef](#)] [[PubMed](#)]
14. Moriya-Sato, A.; Hida, A.; Inagawa-Ogashiwa, M.; Wada, M.R.; Sugiyama, K.; Shimizu, J.; Yabuki, T.; Seyama, Y.; Hashimoto, N. Novel acyl-CoA synthetase in adrenoleukodystrophy target tissues. *Biochem. Biophys. Res. Commun.* **2000**, *279*, 62–68. [[CrossRef](#)] [[PubMed](#)]
15. Fraisl, P.; Forss-Petter, S.; Zigman, M.; Berger, J. Murine bubblegum orthologue is a microsomal very long-chain acyl-CoA synthetase. *Biochem. J.* **2004**, *377 Pt 1*, 85–93. [[CrossRef](#)] [[PubMed](#)] [[PubMed Central](#)]
16. Lopes-Marques, M.; Machado, A.M.; Ruivo, R.; Fonseca, E.; Carvalho, E.; Castro, L.F.C. Expansion, retention and loss in the Acyl-CoA synthetase “Bubblegum” (Acsbg) gene family in vertebrate history. *Gene* **2018**, *664*, 111–118. [[CrossRef](#)] [[PubMed](#)]
17. Jia, Z.; Moulson, C.L.; Pei, Z.; Miner, J.H.; Watkins, P.A. Fatty acid transport protein 4 is the principal very long chain fatty acyl-CoA synthetase in skin fibroblasts. *J. Biol. Chem.* **2007**, *282*, 20573–20583. [[CrossRef](#)] [[PubMed](#)]
18. Fagerberg, L.; Hallström, B.M.; Oksvold, P.; Kampf, C.; Djureinovic, D.; Odeberg, J.; Habuka, M.; Tahmasebpour, S.; Danielsson, A.; Edlund, K.; et al. Analysis of the human tissue-specific expression by genome-wide integration of transcriptomics and antibody-based proteomics. *Mol. Cell. Proteom.* **2014**, *13*, 397–406. [[CrossRef](#)] [[PubMed](#)] [[PubMed Central](#)]
19. Rozen, S.; Skaletsky, H. Primer3 on the WWW for general users and for biologist programmers. *Methods Mol. Biol.* **2000**, *132*, 365–386. [[CrossRef](#)] [[PubMed](#)]
20. Lagerstedt, S.A.; Hinrichs, D.R.; Batt, S.M.; Magera, M.J.; Rinaldo, P.; McConnell, J.P. Quantitative determination of plasma c8-c26 total fatty acids for the biochemical diagnosis of nutritional and metabolic disorders. *Mol. Genet. Metab.* **2001**, *73*, 38–45. [[CrossRef](#)]
21. Jia, Z.; Pei, Z.; Li, Y.; Wei, L.; Smith, K.D.; Watkins, P.A. X-linked adrenoleukodystrophy: Role of very long-chain acyl-CoA synthetases. *Mol. Genet. Metab.* **2004**, *83*, 117–127. [[CrossRef](#)] [[PubMed](#)]
22. Wang, Y.; Yu, W.; Li, S.; Guo, D.; He, J.; Wang, Y. Acetyl-CoA Carboxylases and Diseases. *Front. Oncol.* **2022**, *12*, 836058. [[CrossRef](#)] [[PubMed](#)] [[PubMed Central](#)]
23. Günenc, A.N.; Graf, B.; Stark, H.; Chari, A. Fatty Acid Synthase: Structure, Function, and Regulation. *Subcell. Biochem.* **2022**, *99*, 1–33. [[CrossRef](#)] [[PubMed](#)]
24. A’Bháird, N.N.; Ramsay, R.R. Malonyl-CoA inhibition of peroxisomal carnitine octanoyltransferase. *Biochem. J.* **1992**, *286 Pt 2*, 637–640. [[CrossRef](#)] [[PubMed](#)] [[PubMed Central](#)]
25. Brenna, J.T.; Kothapalli, K.S.D. New understandings of the pathway of long-chain polyunsaturated fatty acid biosynthesis. *Curr. Opin. Clin. Nutr. Metab. Care* **2022**, *25*, 60–66. [[CrossRef](#)] [[PubMed](#)]
26. Wang, X.; Yu, H.; Gao, R.; Liu, M.; Xie, W. A comprehensive review of the family of very-long-chain fatty acid elongases: Structure, function, and implications in physiology and pathology. *Eur. J. Med. Res.* **2023**, *28*, 532. [[CrossRef](#)] [[PubMed](#)] [[PubMed Central](#)]

27. Bezman, L.; Moser, A.B.; Raymond, G.V.; Rinaldo, P.; Watkins, P.A.; Smith, K.D.; Kass, N.E.; Moser, H.W. Adrenoleukodystrophy: Incidence, new mutation rate, and results of extended family screening. *Ann. Neurol.* **2001**, *49*, 512–517. [[CrossRef](#)] [[PubMed](#)]
28. de Beer, M.; Engelen, M.; van Geel, B.M. Frequent occurrence of cerebral demyelination in adrenomyeloneuropathy. *Neurology* **2014**, *83*, 2227–2231. [[CrossRef](#)] [[PubMed](#)]
29. Moser, H.W. Adrenoleukodystrophy: Phenotype, genetics, pathogenesis and therapy. *Brain* **1997**, *120 Pt 8*, 1485–1508. [[CrossRef](#)] [[PubMed](#)]
30. Kemp, S.; Wanders, R. Biochemical aspects of X-linked adrenoleukodystrophy. *Brain Pathol.* **2010**, *20*, 831–837. [[CrossRef](#)] [[PubMed](#)] [[PubMed Central](#)]
31. Sheng, Y.; Tsai-Morris, C.H.; Li, J.; Dufau, M.L. Lessons from the gonadotropin-regulated long chain acyl-CoA synthetase (GR-LACS) null mouse model: A role in steroidogenesis, but not result in X-ALD phenotype. *J. Steroid Biochem. Mol. Biol.* **2009**, *114*, 44–56. [[CrossRef](#)] [[PubMed](#)]
32. Berger, J.; Albet, S.; Bentejac, M.; Netik, A.; Holzinger, A.; Roscher, A.A.; Bugaut, M.; Forss-Petter, S. The four murine peroxisomal ABC-transporter genes differ in constitutive, inducible and developmental expression. *Eur. J. Biochem.* **1999**, *265*, 719–727. [[CrossRef](#)] [[PubMed](#)]
33. Guesnet, P.; Alessandri, J.M. Docosahexaenoic acid (DHA) and the developing central nervous system (CNS)-Implications for dietary recommendations. *Biochimie* **2011**, *93*, 7–12. [[CrossRef](#)] [[PubMed](#)]
34. Dyall, S.C. Long-chain omega-3 fatty acids and the brain: A review of the independent and shared effects of EPA, DPA and DHA. *Front. Aging Neurosci.* **2015**, *7*, 52. [[CrossRef](#)] [[PubMed](#)] [[PubMed Central](#)]
35. Lakshimi, V.I.; Kavitha, M. New Insights into Prospective Health Potential of  $\omega$ -3 PUFAs. *Curr. Nutr. Rep.* **2023**, *12*, 813–829. [[CrossRef](#)] [[PubMed](#)]
36. Nomali, M.; Heidari, M.E.; Ayati, A.; Tayebi, A.; Shevchuk, O.; Mohammadrezaei, R.; Navid, H.; Khayyat-zadeh, S.S.; Palii, S.; Valizade Shiran, F.; et al. Omega-3 supplementation and outcomes of heart failure: A systematic review of clinical trials. *Medicine* **2024**, *103*, e36804. [[CrossRef](#)] [[PubMed](#)] [[PubMed Central](#)]
37. Fathima, S.; Prokopiou, E.; Georgiou, T. Omega-3 Polyunsaturated Fatty Acids and Their Anti-Oxidant, Anti-Inflammatory and Neuroprotective Effects in Diabetic Retinopathy: A Narrative Review. *Front. Biosci.* **2023**, *28*, 153. [[CrossRef](#)] [[PubMed](#)]
38. Schmitz, G.; Ecker, J. The opposing effects of n-3 and n-6 fatty acids. *Prog. Lipid Res.* **2008**, *47*, 147–155. [[CrossRef](#)] [[PubMed](#)]
39. Burdge, G.C. Is essential fatty acid interconversion an important source of PUFA in humans? *Br. J. Nutr.* **2019**, *121*, 615–624. [[CrossRef](#)] [[PubMed](#)]

**Disclaimer/Publisher's Note:** The statements, opinions and data contained in all publications are solely those of the individual author(s) and contributor(s) and not of MDPI and/or the editor(s). MDPI and/or the editor(s) disclaim responsibility for any injury to people or property resulting from any ideas, methods, instructions or products referred to in the content.